ACS OMEGA

http://pubs.acs.org/journal/acsodf

Article

Hybrid Hemp Particles as Functional Fillers for the Manufacturing of Hydrophobic and Anti-icing Epoxy Composite Coatings

Jessica Passaro,* Aurelio Bifulco,* Elisa Calabrese, Claudio Imparato, Marialuigia Raimondo, Roberto Pantani, Antonio Aronne, and Liberata Guadagno

Cite This: *ACS Omega* 2023, 8, 23596−23606

Read Online

ACCESS | Metrics & More | Article Recommendations | Supporting Information

ABSTRACT: The development of hydrophobic composite coatings is of great interest for several applications in the aerospace industry. Functionalized microparticles can be obtained from waste fabrics and employed as fillers to prepare sustainable hydrophobic epoxy-based coatings. Following a waste-to-wealth approach, a novel hydrophobic epoxy-based composite including hemp microparticles (HMPs) functionalized with waterglass solution, 3-aminopropyl triethoxysilane, polypropylene-graft-maleic anhydride, and either hexadecyltrimethoxysilane or 1*H*,1*H*,2*H*,2*H*-perfluorooctyltriethoxysilane is presented. The resulting epoxy coatings based on hydrophobic HMPs were cast on aeronautical carbon fiber-reinforced panels to improve their anti-icing performance. Wettability and anti-icing behavior of the prepared composites were investigated at 25 °C and −30 °C (complete icing time), respectively. Samples cast with the composite coating can achieve up to 30 °C higher water contact angle and doubled icing time than aeronautical panels treated with unfilled epoxy resin. A low content (2 wt %) of tailored HMPs causes an increase of ∼26% in the glass transition temperature of the coatings compared to pristine resin, confirming the good interaction between the hemp filler and epoxy matrix at the interphase. Finally, atomic force microscopy reveals that the HMPs can induce the formation of a hierarchical structure on the surface of casted panels. This rough morphology, combined with the silane activity, allows the preparation of aeronautical substrates with enhanced hydrophobicity, anti-icing capability, and thermal stability.

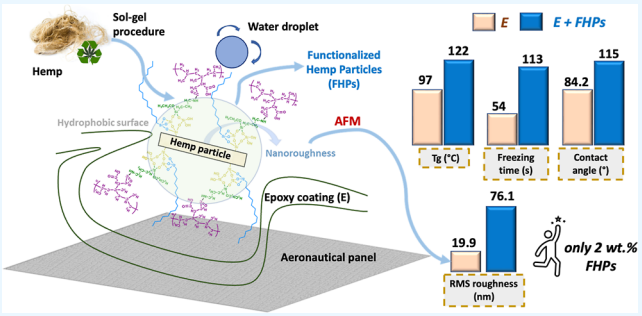

1. INTRODUCTION

In the last decades, superhydrophobic surfaces have drawn great attention both in academia and in industry due to their self-cleaning,[1] anti-icing,[2] antifouling,[3] antifogging,[4] and anticorrosive[5] properties. In particular, superhydrophobic surfaces can be useful in many industrial fields, such as automotive,[6] aerospace,[7] textiles,[8] medical diagnostics, and sensing,[9] plus they can be combined with smart functionalities derived from nanoparticles.[10−12] The surface wettability is determined by the strength of the cohesive forces within the water molecules and the interaction of the water with the surface itself. When water droplets roll off, keeping the surface dry, the cohesive forces within the water molecules are greater than those on the surface.[13] A hydrophobic surface provides a water contact angle (CA) larger than 90°, while a superhydrophobic surface exhibits a water CA larger than 150° and a contact angle hysteresis (CAH) lower than 10°.[14] Low surface energy and micro-/nano-hierarchical roughness of the solid substrate are the two fundamental parameters for designing a superhydrophobic surface.[13] Inorganic oxide nanoparticles (e.g., silica, zinc oxide, titania) can provide rough surfaces with a microscale/nanoscale architecture.[15−18] For the development of the hydrophobic/superhydrophobic coatings, different fabrication techniques can be utilized, for example, electrochemical deposition,[19] electro-spinning and electro-spraying,[20,21] chemical vapor deposition,[22] layer-by-layer deposition,[23] sol−gel processing, and solution casting.[24,25] Among these, the sol−gel method and water glass route are widely used, as they operate under mild and low-cost conditions to produce a variety of nanostructured materials[26,27] and superhydrophobic layers on various substrates.[24,28] Superhydrophobic coatings derived from silica sols and hydrophobic compounds have been widely investigated. Silica can be functionalized by alkyl silanes and fluorinated alkyl silanes, obtaining hydrophobic and superhydrophobic coatings showing low surface free energy owing to the surface hydroxyl groups.[29−32] Among hydrophobic compounds, the fluorinated ones exhibit high effectiveness; however, they have some drawbacks, including high costs and risks for human health and

Received: March 2, 2023
Accepted: April 24, 2023
Published: June 16, 2023

Scheme 1. Overall Procedure for the Synthesis of Hydrophobic Hemp Particles

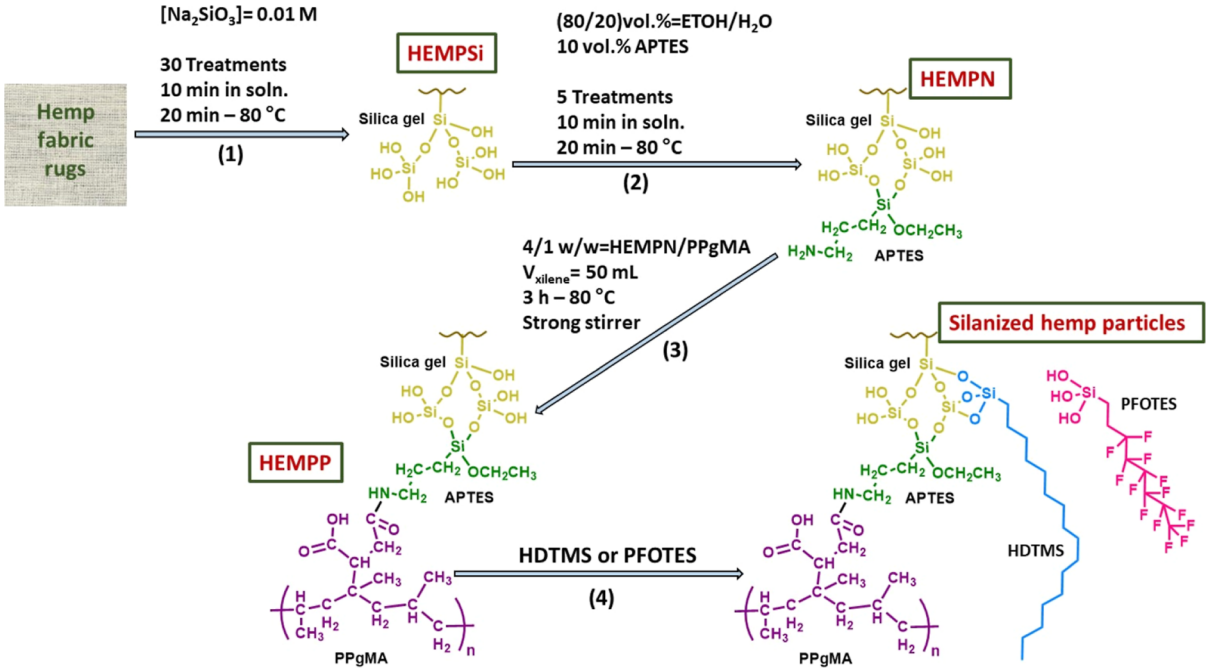

the environment.[33,34] The US Environmental Protection Agency and the European Chemicals Agency are considering the restriction of several long-chain linear per- and polyfluoroalkyl substances (PFAS).[35,36] Nevertheless, PFAS are still widely used as functional additives to prepare hydrophobic products. Hence, the use of non-fluorinated silanes, such as long-chain alkyl silanes, is encouraged for fabricating sustainable coatings owing to their lower toxicity and low costs.

Epoxy resins have been widely used as a matrix to prepare hydrophobic nano-/micro-composite coatings[37−39] due to their easy processing, strong adhesion to many substrates, and excellent chemical resistance.[40] The high surface energy of epoxy resins strongly limits their use as the polymer matrix in the manufacturing of water-proof coatings. To overcome such limitations, it is possible to disperse hydrophobic nanoparticles into the epoxy matrix,[41−43] before applying the coating onto a substrate (e.g., carbon fiber panels, plastic films, glass slides, metals, etc.).[44−47] Recently, natural fibers have become more attractive as potential sustainable and eco-friendly reinforcement for epoxy composites, encouraging the use of surplus cellulose fibers derived from agricultural waste.[48,49] However, due to their hydrophilic chemical nature, the use of cellulose-based particles as platforms and functional fillers for the manufacturing of hydrophobic epoxy-based coatings has not yet been investigated. The few works on the wettability of epoxy composites containing natural microfibers reported an unaltered[50] or decreased[51] hydrophobic character. Moreover, the treatment of jute fibers with an epoxy resin solution caused only a slight increase in water CA (from about 67° to 74°),[52] confirming that offsetting the marked hydrophilicity of these materials is a challenging task. In the context of the circular economy, the production of modified hemp particles would represent a sustainable and easy solution for the recovery of waste hemp rugs, as epoxy resins and fabrics are largely used in the aerospace sector for the fabrication of multifunctional fiber-reinforced composites.[53,54] In this perspective, it would be highly desirable to exploit properly functionalized hemp-based particles as fillers for manufacturing composite coatings with enhanced hydrophobicity and anti-icing performances without any detrimental impact on the viscoelastic behavior and the thermal stability of the polymer matrix.

In the present study, hydrophobic composite epoxy coatings were cast onto typical aeronautical panels, based on carbon-fiber-reinforced (CFR) polymers, to assess their feasibility in aerospace applications. In particular, the possibility of obtaining innovative fiber-reinforced epoxy coatings reusing waste hemp as particles, functionalized with waterglass (i.e., sodium metasilicate) solution, 3-aminopropyl triethoxysilane (APTES), polypropylene-*graft*-maleic anhydride (PPgMA) and silanes, either hexadecyltrimethoxysilane (HDTMS) or 1*H*,1*H*,2*H*,2*H*-perfluorooctyltriethoxysilane (PFOTES), was deeply investigated, and the influence of the molecular structure of these silanes on the wettability and anti-icing performances of treated aeronautical panels was evaluated. Through this approach, hemp particles' surface chemistry and morphological characteristics can improve the interphase between the filler and the polymer matrix and confer rough morphology to the surface, leading to a higher glass transition temperature and reduced wettability compared to the virgin epoxy coating.

2. EXPERIMENTAL SECTION

2.1. Materials. CFR panels with a size of 7.5 × 2.5 × 0.1 cm^3 have been used as substrates. CFR panels are commonly used as structural materials in the manufacturing of aircraft and their components. The hemp fabric rugs were supplied by MAEKO S.r.l. (Milan, Italy). Sodium metasilicate (Na_2SiO_3, waterglass), APTES (>98%), hydrochloric acid (37 wt %), PPgMA with 8−10 wt % maleic anhydride content and an average M_w ∼ 9100 by gel permeation chromatography (GPC), HDTMS (>85%), and PFOTES (98%) were purchased from Sigma-Aldrich (Merck KGaA, Darmstadt, Germany). A two-component epoxy resin system (SX10),

https://doi.org/10.1021/acsomega.3c01415
ACS Omega 2023, 8, 23596−23606

consisting of a modified diglycidyl ether of bisphenol-A (DGEBA) resin and isophorone diamine (IDA), a cycloaliphatic diamine hardener, purchased from MATES S.r.l. (Milan, Italy), was used for the preparation of the polymer matrix in the composite coatings.

2.2. Methods. *2.2.1. Synthesis and Functionalization of Hemp Fabric Microparticles.* Hemp fabric rugs are generally used in the manufacturing of fiber-reinforced epoxy composites and are one of the most abundant waste materials resulting from the fabrication process. In Scheme 1, the overall procedure for the synthesis of hydrophobic hemp particles is shown.

Starting from waste hemp fabric rugs, HMPs were obtained through a sol−gel route previously established.[55,56] Briefly, hemp fabric rugs were submitted to iterated soaking−drying cycles (see stage 1 of Scheme 1) in a waterglass (Na_2SiO_3, 0.01 M) solution acidified up to pH = 2.5 with hydrochloric acid (HCl). The sol−gel methodology allows for the deposition of a silica gel on the surface of hemp rugs, which makes them brittle after drying.[56] Then, the dry fabrics could be reduced to silica-coated hemp powder (HEMPSi) particles by a low-power (350 W) mixer (IMETEC S.p.A., Azzano San Paolo, Bergamo, Italy). In the second step (see stage 2 of Scheme 1), the functionalization with amino groups was performed by laying HEMPSi particles in an EtOH/water solution acidified up to pH = 5 with acetic acid and containing APTES. The final product (HEMPN) was washed with an EtOH/water solution through centrifugation cycles.[55]

In the present study, to confer hydrophobic character to HEMPN microparticles, the following strategy was adopted. The primary amino groups were left to react with maleic anhydride molecules grafted along polypropylene chains of PPgMA (see stage 3 of Scheme 1). For a typical synthesis, this reaction was performed as follows: 0.25 g of PPgMA was added into a vessel containing 50 mL of xylene solution at 80 °C and left stirring till the complete dissolution of the polypropylene-based compatibilizer. Then, 1 g of HEMPN particles, fully dried overnight at 60 °C, was added to the vessel and left reacting under reflux for 3 h at 80 °C. The final product (HEMPP) was washed with pure xylene by three centrifugation cycles to remove unreacted PPgMA and finally with a solution of EtOH/water (80:20 v/v %).[57]

2.2.2. Manufacturing of Fiber-Reinforced Epoxy Coatings. The bulk sample of blank epoxy (EPO) was manufactured by mixing a certain amount of unfilled DGEBA with an amine hardener (26 wt % of the epoxy resin). After stirring at room temperature, the mixture was poured into a silicone rubber mold (5 × 5 × 0.3 cm^3), with a thickness of 0.1 cm, cured at 60 °C for 24 h, and then post-cured at 80 °C for 4 h. By following a similar procedure, functionalized HMPs were used to fabricate DGEBA-based epoxy composite coatings with the same dimensions (5 × 5 × 0.1 cm^3). In the preparation of a typical formulation, a specific amount of DGEBA resin was added with 2 wt % of HEMPP particle loading (this content was selected on the basis of tan δ measurements previously performed on a similar system by some of the authors[55]), 10 wt % of acetone, and 1 wt % of HDTMS or PFOTES (see stage 4 of Scheme 1) silanizing agent. These percentage values for the synthesis all refer to the epoxy matrix cured with 26 wt % of hardener. These bulk composite coatings were cured at the same conditions as the EPO sample.

The unfilled epoxy coating and composite ones were also deposited by the drop-casting method from one-pot formulations on aeronautical panels based on the carbon fiber-reinforced material. Before the deposition, the formulations were strongly stirred to obtain homogeneous systems and then weakly sonicated to remove the bubbles. The final products were cast on CFR panels (7.5 × 2.5 × 0.1 cm^3) previously cleaned with ethanol. The coated substrates were cured at 60 °C for 24 h and then post-cured at 80 °C for 4 h. Untreated CFR panels and coated ones are shown in Figure S1. It can be observed that the deposition of the coatings does not alter the chromatic characteristics of the substrates, confirming a uniform distribution of the filler at a macroscopic scale. In the next sections, the epoxy coating samples containing HEMPP particles modified with HDTMS and PFOTES will be named EH_HDTMS and EH_PFOTES, respectively.

2.2.3. Wettability and Anti-icing Tests. The **wettability** of composite coatings was evaluated by measuring the CA and the CAH. The CA measurement allows the evaluation of the surface interaction of the investigated system with three phases (solid, liquid, and vapor). The CA is the angle arising from the intersection of liquid−vapor and solid−liquid interfaces (see Figure S2a).[58] This angle forms when a liquid drop lies on a horizontal plane. The CA of distilled water was evaluated by a high-resolution camera (iPhone 13 Pro Max-12 MP, f/1.5, 26 mm-12 MP, f/2.8, 77 mm-12 MP, f/1.8, 13 mm-LiDAR ToF 3D, Apple Inc.) at room temperature using the sessile drop method.[58] The CA was measured with an open-source image processing software ImageJ (v.1.52t, NIH, 2020). The CAH was evaluated as follows: a distilled water drop was placed on the substrate, firmly anchored to an inclined plane, and the CAs (advancing and receding) were collected when the droplet started sliding down (Figure S2b). The difference between the advancing (θ_A) and receding (θ_R) contact angles corresponds to the CAH (eq 1).

$$\mathrm{CAH} = \theta_A - \theta_R \tag{1}$$

All the CAs were estimated by placing water drops of volume in the range of 30−40 μL on the coating surface with a micropipette.

The **anti-icing** test was performed by dripping water droplets (30−40 μL) on the surfaces of overcooled samples (−30 °C).[2] First, the samples were placed in a refrigerator at a temperature of −30 °C for 10 min. Then, the deionized water droplet was dripped onto the coating's surface. Meanwhile, a high-speed camera (pco. dimax cs1, PCO) was used for recording the freezing process. Figure S3 shows the apparatus used for the anti-icing tests.

2.2.4. Structural, Morphological, and Thermal Analysis. 2.2.4.1. Attenuated Total Reflectance−Fourier Transform Infra-Red. Attenuated total reflectance−Fourier transform infra-red (ATR−FTIR) analysis was performed on the functionalized HMPs and epoxy coatings by using a Nicolet 5700 spectrometer (Thermo Fisher, Waltham, MA, USA) with a single reflection ATR accessory. The instrument has a resolution of 4 cm^{-1}, and the collected spectra was the result of 32 running scans. The analysis software used was Thermo Scientific OMNIC Software Suite (v7.2, Thermo Fisher, Waltham, MA, USA, 2005).

2.2.4.2. Atomic Force Microscopy. Atomic force microscopy (AFM) analysis was performed by means of a Bruker NanoScope V multimode AFM (Digital Instruments, Santa Barbara, CA, USA) apparatus to quantify the surface roughness parameters and analyze the nanoscale surface morphology of

https://doi.org/10.1021/acsomega.3c01415
ACS Omega 2023, 8, 23596−23606

samples EPO, EH_HDTMS, and EH_PFOTES. Topographic height images were acquired at room temperature and processed using a Bruker software Nanoscope Analysis 1.80 (BuildR1.126200). The measurements were performed in tapping mode, in which the sharp tip of the probe scans the sample surface intermittently by oscillating up and down as the cantilever is vibrated near its resonance frequency. The tip is characterized by a radius of 5−10 nm, a nominal spring constant of 20−100 N/m, and resonance frequencies of 200−400 kHz. For each analyzed sample, several AFM images were acquired at different locations to evaluate the trend of the roughness parameters and verify if these are reproducible on different scanned areas of the samples. The scanning rate was 0.500 Hz per scan line, with 512 pixels per line. In order to evaluate the surface roughness, different roughness parameters are generally estimated and applied. The magnification of the scanned area during the AFM acquisition greatly influences the roughness parameters. This means that the roughness value measured for a large section of the surface will be very different from that calculated for a smaller section. In fact, AFM images having the same scan size were compared for the three samples EPO, EH_HDTMS, and EH_PFOTES in order to effectively quantify the roughness values. In this work, to derive the quantitative roughness, two of the most relevant height parameters, namely, the roughness average (R_a) and the root mean square roughness (R_q), have been considered. More precisely, R_a represents the arithmetic mean of the absolute values of the height of the surface profile, and R_q is analogous to the roughness average (R_a), with the only difference that R_q is more sensitive to peaks and valleys than R_a, due to the squaring of the amplitude in its calculation. These amplitude parameters, which characterize the surface based on the vertical deviations of the roughness map from the mean surface, are extensively used in the literature.[59,60] For all the samples, the R_a and R_q parameters were evaluated according to eqs 2 and 3

$$R_a = \frac{1}{l_r}\int_0^{l_r} |z(x)| \times dx \quad (2)$$

$$R_q = \sqrt{\frac{1}{l_r}\int_0^{l_r} z(x)^2 dx} \quad (3)$$

where l_r is the length of the line, z is the height, and x is the position.

The surface morphology of the functionalized HMPs and coated aeronautical panels was observed via scanning electron microscopy (SEM) using a Leica Stereoscan 440 microscope (20 kV) (Cambridge Ltd., Cambridge, UK), coupled with an energy-dispersive X-ray (EDX) analytical system (Inca Energy 200). The Aztec Energy EDS software (v2.1, Oxford Instruments, Abingdon, UK, 2006) was used.

2.2.4.3. Scanning Electron Microscopy. SEM of hemp particles was performed at each functionalization step using a Leica Stereoscan 440 microscope (20 kV) (Leica Microsystems Cambridge Ltd., Cambridge, UK), coupled with an EDX system (Inca Energy 200). The EDX system used an Aztec Energy EDS Software (v2.1, Oxford Instruments, Abingdon, UK, 2006).

2.2.4.4. Differential Scanning Calorimetry. Differential scanning calorimetry (DSC) was carried out to evaluate the thermal behavior of EPO, EH_HDTMS, and EH_PFOTES samples. The analysis was performed by a Mettler DSC 822/400 thermal analyzer (Mettler-Toledo Columbus, OH, USA) at a heating rate of 10 °C/min by running two repeating cycles (from 20 °C to 300 °C) under a N_2 flow (50 mL/min). The T_g value was determined at the inflection point on the second heating curve.

2.2.4.5. Thermogravimetric Analysis. Thermogravimetric analysis (TGA) was performed on a Mettler TGA/SDTA 851 (Mettler-Toledo Columbus, OH, USA) instrument under air and N_2 atmospheres with a flow rate of 50 mL/min. The weight loss as a function of the temperature was recorded at 10 °C/min from 25 °C to 800 °C.

3. RESULTS AND DISCUSSION

3.1. Structural Analysis of Functionalized Hemp Particles and Epoxy Composite Coatings. It is known that the hydrophobicity of a surface depends on two main effects: the texture morphology of the surface and its chemistry. A polymer coating exhibiting a micro-structured surface is more hydrophobic than a flat surface.[61] Hence, to make hemp particles a suitable functional filler for lowering the wettability of epoxy-based coatings, their surface chemistry needs to be modified to increase their hydrophobicity and affinity toward the polymer matrix. HEMPSi powders were composed of microparticles of diameter ranging from tens of nanometers to tens of microns, as shown by SEM images (Figure 1a).[55] Such a morphology derives from the web-like structure formed by the fibrils and microfibrils of hemp.[57,62]

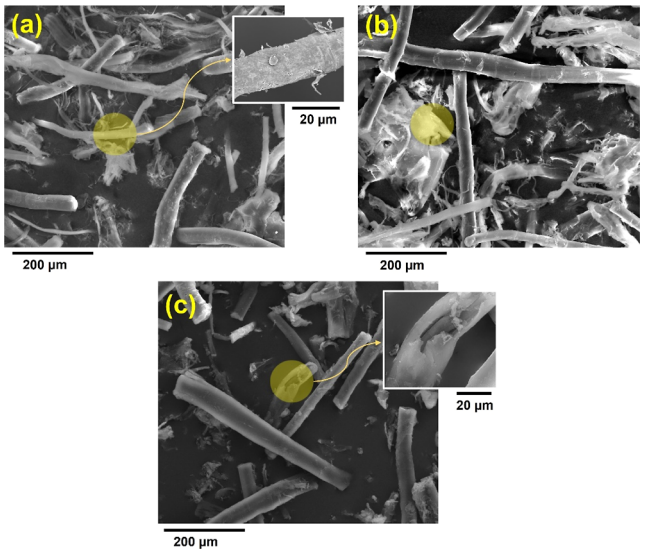

Figure 1. SEM micrographs at different magnifications of (a) silica gel-functionalized hemp particles (HEMPSi), (b) amino-functionalized hemp particles (HEMPN), and (c) HEMPN particles functionalized with PPgMA. The yellow circles indicate the areas where EDX analysis was performed.

The analysis of the ATR−FTIR spectrum of the HEMPSi sample reveals the presence of a layer of silica gel rich in silanol groups, as attested by the broad bands at about 3340 cm^{-1} (ν_{O-H}) and 1100 cm^{-1} (ν_{Si-O}) (Figure S4). The formation of a silicon-based layer is confirmed by EDX analysis (Table 1). Silanol groups on the surface of HMPs can react through condensation with APTES, a well-known coupling agent for epoxy systems.[63,64] Figure 1b reports SEM images of amino-functionalized hemp particles (HEMPN). The presence of

https://doi.org/10.1021/acsomega.3c01415
ACS Omega 2023, 8, 23596−23606

Table 1. Elemental Analysis (EDX) of Surface Chemical Composition (wt %) of Functionalized Hemp Particles

composition (%)	C	O	N	Si
HEMPSi	39.5	57.3		3.2
HEMPN	37.9	53.2	6.7	2.2
HEMPP	46.5	45.6		7.9

primary amino groups on these fibers is clearly shown by the appearance of IR bands at 1554 cm^{-1} (δ_{N-H}) and 1407 cm^{-1} (ν_{C-N}) (see Figure S4) and is confirmed by EDX measurements (Table 1), which reveal a significant amount of nitrogen on the hemp surface. The amino groups on HEMPN particles can react with the oxirane rings of the epoxy chain; therefore, the resulting material can be used to prepare fiber-reinforced epoxy composites with tailored interphase. However, as observed in a previous work,[55] HEMPN particles tend to segregate in the polymer matrix as their surface chemistry limits the migration of such fillers to the surface of epoxy coatings. Conversely, PPgMA-functionalized (HEMPP) particles show a non-polar character and are not able to react with oxirane rings. SEM micrographs at different resolutions (Figure 1c) reveal that HEMPP particles still exhibit the characteristic unregular rugged morphology,[57,62] and their surface appears slightly waxy and different compared to the ones of HEMPSi and HEMPN samples. This may be ascribed to a thin layer of PP covering the primary wall of hemp particles. The presence of this polymer coating is further supported by a higher amount of carbon recorded by EDX investigation for HEMPP particles with respect to HEMPSi (Table 1). It also makes nitrogen undetectable by EDX, probably because the nitrogen signal is covered by PPgMA after the reaction of primary amino groups with maleic anhydride moieties.[57,62] The successful grafting of PPgMA on the surface of the final product (HEMPP) is assessed by the characteristic bands attributed to C−H bending at 1376 cm^{-1} (ρ_{CH3}) and 1460 cm^{-1} (δs_{CH2}) and by the increase of the C−H stretching bands in the region 2900−3000 cm^{-1} (Figure S4).

The functionalization of hemp particles by PPgMA completely changes the chemical characteristics of their surface, enhancing their hydrophobicity and causing them to appear much more similar to the epoxy resin from a chemical point of view. Thus, due to their chemical and morphological characteristics, HEMPP particles appear highly suitable to be incorporated into epoxy systems to manufacture polymer coatings with hierarchical micro-structured surface textures. To combine this aspect with an even more hydrophobic chemistry for HEMPP, these particles were additionally functionalized with two silanes with non-polar chains, HDTMS and PFOTES (see Scheme 1). As shown in Table 1, HEMPP particles display a residual amount of silicon on their surface due to some free silanol groups that have remained unreacted. These silanol groups can condensate with HDTMS and PFOTES (see Scheme 1) during the curing process (cure: 60 °C/24 h, post-cure: 80 °C/4 h) to form tailored hemp particles with a rugged morphology, high hydrophobicity, and enhanced compatibility with the epoxy matrix.[65,66]

The chemical structure of the pristine epoxy resin (EPO) and the composites containing the functionalized hemp particles (EH_HDTMS and EH_PFOTES) was investigated by ATR−FTIR spectra (Figure S5). All the samples appear completely cured, as attested by the disappearance of the oxirane ring vibration band at 913 cm^{-1} and by the rise of the O−H stretching band between 3500 and 3100 cm^{-1}.[67−69] It is known that the position of this band is very sensitive to the strength of H-bonding in which OH groups are involved, shifting toward lower frequency and increasing the magnitude of H-bonding.[70] For pure epoxy, two features at about 3470 and 3322 cm^{-1} are seen, which can be related to free and H-bonded hydroxyls, respectively. For the EH_HDTMS and EH_PFOTES composites, the O−H stretching band shows a single feature at about 3380 cm^{-1}, indicating weaker H-bonding interactions between the epoxy matrix and the functional groups of hemp particles.[68,71] Furthermore, in the spectra of EH_HDTMS and EH_PFOTES, despite the low concentration of both HEMPP particles and silanes, some of their main functional groups can be detected, for example, the Si−O bonds, whose stretching lies between 1030 and 1080 cm^{-1}, while other features are overlapped with the several characteristic vibrations of the polymer matrix.

3.2. Wettability and Anti-icing Properties. The water CA and CAH values of the uncoated and treated aeronautical panels are displayed in Table 2 and Figure 2. The intrinsic

Table 2. Wettability and Anti-icing Parameters of Untreated and Coated CFR Panels: CA, CAH, and Freezing Time[a]

sample	CA (deg)	CAH (deg)	freezing time (s)
panel	62 ± 3		35 ± 5
EPO	84 ± 2	55 ± 3	54 ± 2
EH_HDTMS	96 ± 3	43 ± 2	78 ± 3
EH_PFOTES	115 ± 3	33 ± 4	113 ± 5

[a]CAH was not measured for the pristine panel as the droplet could not slide down.

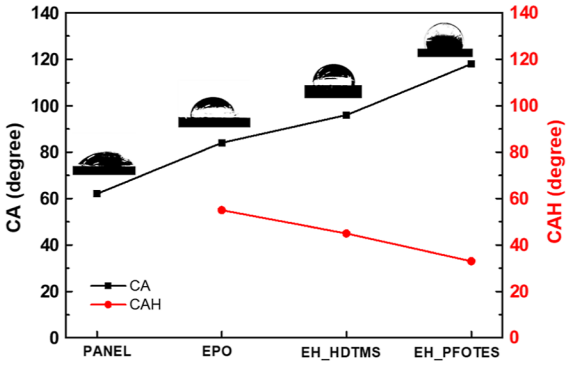

Figure 2. CA, CAH, and water droplet representations of untreated and coated CFR panels.

water CA value of the pristine substrate was 62° ± 3°, which denotes a hydrophilic behavior of the carbon fiber-reinforced panel. In coated samples, in the absence of a functionalized hemp filler, the deposition of EPO does not change the hydrophilic character (water CA = (84° ± 2°) < 90°). This hydrophilicity can be explained by the presence of hydroxyl groups, arising from the curing of the resin, which can form H-bonds with water molecules,[72] as confirmed by the ATR−FTIR investigation. A slight hydrophobicity (water CA = (96° ± 3°) > 90°) is observed for the EH_HDTMS coating. As previously demonstrated, HEMPP particles still exhibit free silanol groups, making them amphiphilic and able to migrate to the surface of the epoxy matrix, establishing a micro-structured and rough texture (see Section 3.4). The functionalization of hemp particles with PPgMA plays a key role in the above-

https://doi.org/10.1021/acsomega.3c01415
ACS Omega 2023, 8, 23596−23606

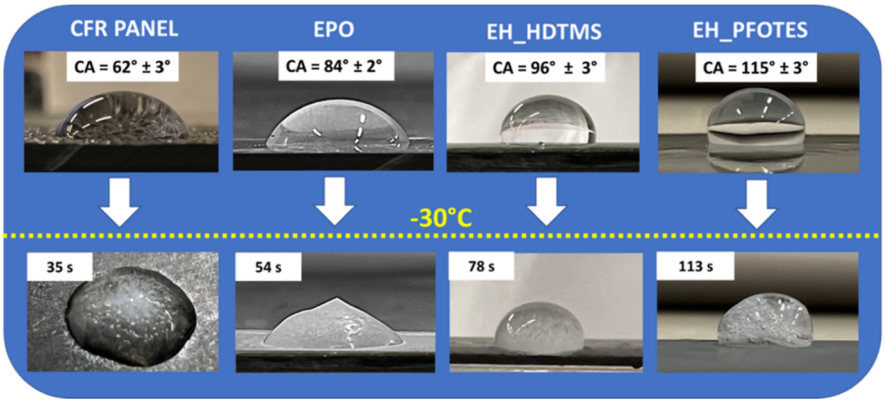

Figure 3. Photographs of water droplets frozen at −30 °C (under the yellow dot line), water CAs, and freezing time of water droplets on bare CFR panels and substrates treated with pristine resin (EPO), EH_HDTMS, and EH_PFOTES coatings.

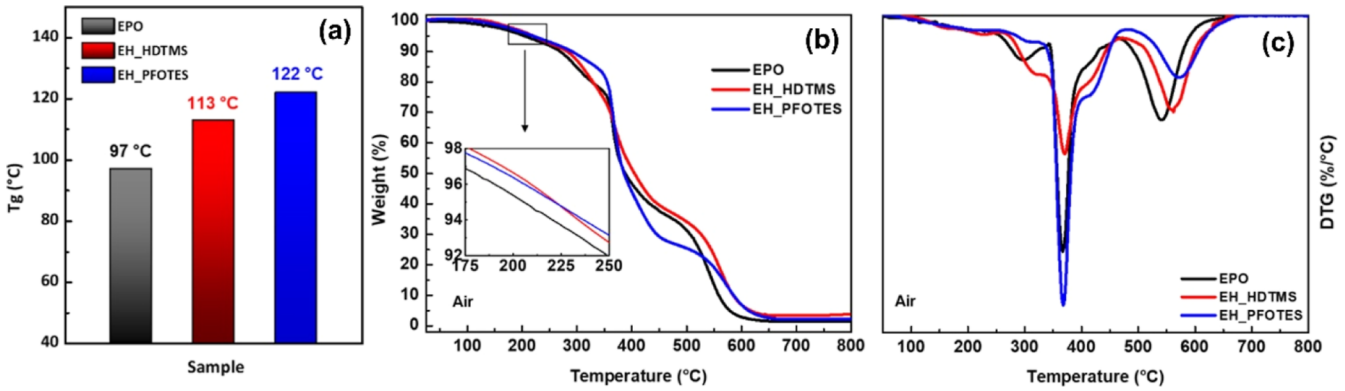

Figure 4. (a) Histogram of T_g values from DSC analysis and (b) TGA and (c) DTG graphics of EPO, EH_HDTMS, and EH_PFOTES samples in the air atmosphere.

described migration phenomenon and, at the same time, increases the hydrophobicity of the surface and the compatibility with the polymer matrix. The anchoring of HDTMS causes the exposure of alkyl chains at the solid−air interface, which, combined with the suitable morphology, provides higher CA and lower CAH than EPO (see Table 2). Concerning the panel coated with EH_PFOTES, the presence of fluorinated alkyl chains boosts the hydrophobic response of the surface [water CA = (115° ± 3°), see Table 2 and Figure 2], due to the well-known function of fluorine-based silanes in lowering the wettability of coatings.[13] Figure 2 shows the progressive increase in CA and a relative decrease in CAH moving from EPO to EH_PFOTES, highlighting the effects of structural and chemical contributions on surface wettability. The rough morphology and non-polar character of the functionalized hemp particles exert a synergistic action in enhancing the hydrophobicity of the epoxy composite coatings, even using a low content of the waste-derived filler (2 wt %) in a simple one-pot procedure with mild operating conditions.

The potential effectiveness of epoxy composite coatings as protective layers against ice formation was evaluated by measuring the freezing time of water droplets deposited on the surfaces of the aeronautical panels at −30 °C. Figure 3 shows the shape of the droplets as deposited at room temperature and their change after the freezing process on pristine CFR panels and substrates coated with pure epoxy (EPO), EH_HDTMS, and EH_PFOTES coatings.

The water droplets on the CFR panel and on EPO were semicircular in shape and froze within 35 and 54 s, respectively. In contrast, the water droplet on the EH_HDTMS and EH_PFOTES coatings remained more spherical due to the higher hydrophobicity, and the freezing time was delayed up to 113 s (see Table 2 and Figure 3). These results can be explained by the reduction of the contact area between the water droplet and the hydrophobic surface, which leads to a lower heat transfer rate.[73−75] The increase of CA and reduction of CAH values caused by the presence of the silanized hemp particles in the epoxy coatings (EH_HDTMS and EH_PFOTES) are clearly related to the anti-icing performances, as the observed variation of these parameters agrees with a reduced ice adhesion strength on the coated panels.[76,77] Based on the values of the collected CAs, the formation of ice on EH_HDTMS and EH_PFOTES coatings occurs by a heterogenous nucleation mechanism.[78] This low adhesion, combined with the decreased contact area, increases water droplet freezing time. Although PFOTES appears to be the most effective functionalizing agent, HDTMS represents a valuable greener alternative, still improving wettability and anti-icing properties.

3.3. Thermal Analysis. DSC analysis was performed to investigate the thermal behavior of the epoxy composite coatings (EPO, EH_HDTMS, and EH_PFOTES). Figure S6 shows the DSC curves collected at the second heating run, and Figure 4a reports the estimated glass transition temperature (T_g) values for each sample. The absence of exothermic phenomena in DSC thermograms proves that all the coatings

https://doi.org/10.1021/acsomega.3c01415
ACS Omega 2023, 8, 23596−23606

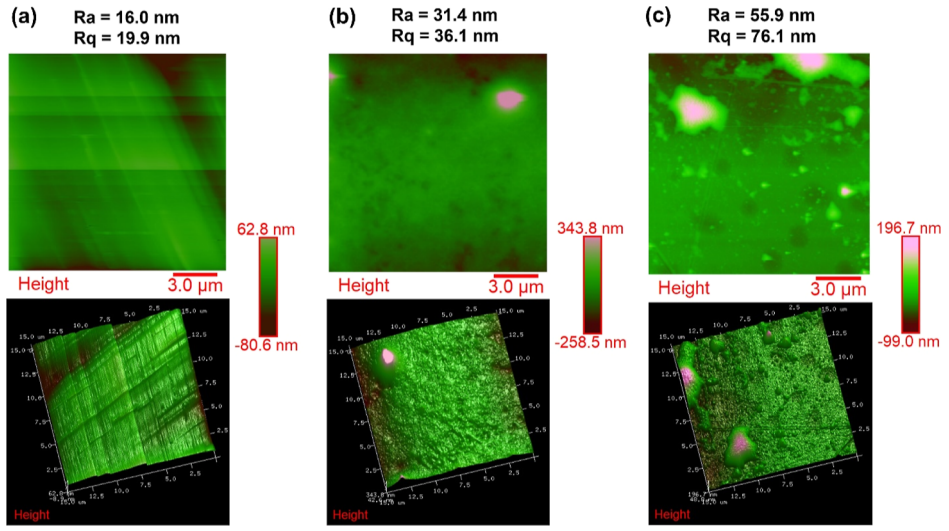

Figure 5. AFM 2D and 3D pictures of CFR panels coated with (a) EPO, (b) EH_HDTMS, and (c) EH_PFOTES.

are fully cured. Thus, the addition of the functionalized hemp particles does not impair the crosslinking process. These results agree with ATR−FTIR measurements. Despite the low amount (2 wt %) of hemp particles, EH_HDTMS and EH_PFOTES exhibit higher T_g values (up to ∼26%) than EPO. The positive effect on the T_g of epoxy coatings is probably due to the chemical functionalization of hemp particles, which makes the interphase between the polymer matrix and filler well-tailored. The non-polar character of silanized hemp particles guarantees their uniform distribution in the matrix, while their surface functional groups allow for the establishment of secondary interactions (e.g., hydrogen bonds) with the epoxy chains, increasing the rigidity of the polymer network.[68] These effects have already been observed with other kinds of fillers, where the instauration of strong non-covalent bonds led to higher T_g values compared to virgin polymeric systems.[79,80] These results suggest that silanized hemp particles could be promising for manufacturing fiber-reinforced epoxy coatings with good mechanical behavior.

The thermo-oxidative stability of epoxy composite coatings has been evaluated by TGA. The TGA and DTG profiles are shown in Figure 4b,c, and the temperatures at the main degradation steps are reported in Table S1. The decomposition of EPO, EH_HDTMS, and EH_PFOTES coatings occurs in two main stages, namely, a first step between 350 °C and 400 °C and a second one around 550 °C, in agreement with the thermal behavior of DGEBA-based systems cured with amine hardeners.[81,82] The presence of physical interactions between the epoxy matrix and the chemically modified hemp fillers increases the initial degradation temperature of the resin by ∼20 °C, as highlighted in the inset of Figure 4b. This result further confirms the formation of secondary bonds in the polymer network,[68] in agreement with ATR−FTIR analysis and T_g values. Besides, EH_HDTMS and EH_PFOTES undergo the second degradation step at temperatures (T_{max2}) up to 30 °C higher than EPO. The T_{max2} values, together with the higher residual masses of the composite samples, prove that the addition of silanized hemp particles into the epoxy matrix allows the production of a more resistant char toward oxidative decomposition and, consequently, an enhanced thermal stability in the air atmosphere.

3.4. Surface Roughness Study. Knowledge of the surface texture represents a crucial aspect of understanding the nature of the material's surface. It is essential to verify the effectiveness of the adhesion at the interface between the polymer matrix and the filler particles. Hydrophobicity is a property that depends on the microstructure of the surface and, more precisely, on its roughness.[83] AFM was used to evaluate the surface roughness of CFR panels coated with the developed epoxy composites and their nanoscale surface morphology. In particular, the measurement of the surface roughness allows assessing the differences in the roughness of each coated sample, even if the deposition method is the same for all investigated samples. AFM measurements also shed light on the influence of the support roughness on the texture of the protective coating. In this work, AFM analysis was used to prove the relationship between the surface roughness of the samples and their hydrophobicity, as demonstrated through the wettability and anti-icing tests (Section 3.2).

Figure 5 shows the representative AFM 2D and 3D topographic pictures corresponding to EPO, EH_HDTMS, and EH_PFOTES coatings, where a surface of 15 μm × 15 μm was scanned in 512 lines. The AFM images show that the nanoscale roughness of the EPO sample is relatively low, as attested by the evaluated roughness parameters R_a = 16.0 nm and R_q = 19.9 nm (Figure 5a). By contrast, both EH_HDTMS and EH_PFOTES samples have a much higher roughness, exhibiting the roughness values R_a = 31.4 nm and R_q = 36.1 nm (Figure 5b) and R_a = 55.9 nm and R_q = 76.1 nm (Figure 5c), respectively. These results perfectly agree with the wettability and anti-icing properties as the surface roughness increases as the CA increases and the CAH decreases. The higher nanoscale roughness shown by EH_HDTMS and EH_PFOTES samples is attributable to the presence of hydrophobic hemp fibers characterized by a rough, irregular morphology of the primary wall surface. With respect to EPO and EH_HDTMS, the EH_PFOTES sample presents a rougher texture due to the higher capability of HEMPP particles functionalized with PFOTES to migrate toward the surface and thus provide it with a more pronounced hierarchical structure. In summary, the roughness parameters corroborate the results from morphological and wettability analysis, evidencing that the proposed methodology allows employing a small amount

https://doi.org/10.1021/acsomega.3c01415
ACS Omega 2023, 8, 23596−23606

of waste-derived fabrics for manufacturing coatings for aeronautical panels showing significant hydrophobicity and antifreeze capacity.

4. CONCLUSIONS

The current study focuses on the possibility of using functionalized particles based on waste hemp to obtain hydrophobic epoxy coatings for aeronautical carbon fiber-reinforced laminates. The proposed chemical modification procedure allows turning an intrinsically hydrophilic material, such as hemp, into hydrophobic particles suitable as fillers in a non-polar polymer matrix to give rise to surfaces with reduced wettability. It was found that, by embedding the functionalized HMPs within the epoxy matrix, a great improvement in terms of thermal behavior, hydrophobicity, and anti-icing performance could be achieved. In particular, the incorporation of only 2 wt % of silane-modified hemp particles into the epoxy resin resulted in both an increased glass transition temperature (up to ∼26%) and an enhanced thermo-oxidative stability because of the good chemical affinity between the functionalized fiber particles and the polymer matrix. Aeronautical panels treated by the composite epoxy coatings exhibited water CA up to 115° and a freezing time of 1.8 min, unlike samples cast with pristine resin showing ∼84° and 0.9 min, respectively. AFM analysis of casted aeronautical laminates proved that the presence of hemp fillers in the epoxy coating led to a rougher surface morphology with a hierarchical structure. The boosted hydrophobicity and anti-icing properties are due to the synergistic effects of chemical and morphological features of the microparticles with anchored silanes. Furthermore, these properties can be tuned using either the high-performing fluorinated silane (PFOTES) or the greener and cheaper alkyl silane (HDTMS). This research may inspire the design and development of sustainable multifunctional composite epoxy coatings containing waste-derived fibers as fillers for aircraft components.

Supporting InformationPhotographs of CFR panels bare and treated with coatings of pristine resin (EPO), EH_HDTMS, and EH_PFOTES; schematic representation of water drop on a plane; schematic of the apparatus used for the anti-icing tests; ATR-FTIR spectra; results of TGA in air atmosphere for pristine resin and epoxy composites; and DSC curves for the samples EPO, EH_HDTMS, and EH_PFOTES (PDF)

■ ASSOCIATED CONTENT

Supporting Information

The Supporting Information is available free of charge at https://pubs.acs.org/doi/10.1021/acsomega.3c01415.

(PDF)

■ AUTHOR INFORMATION

Corresponding Authors

Jessica Passaro − *Department of Industrial Engineering (DIIN), University of Salerno, 84084 Fisciano, Salerno, Italy*; Email: jpassaro@unisa.it

Aurelio Bifulco − *Department of Chemical, Materials and Production Engineering (DICMaPI), University of Naples Federico II, 80125 Naples, Italy*; orcid.org/0000-0002-4214-5385; Email: aurelio.bifulco@unina.it

Authors

Elisa Calabrese − *Department of Industrial Engineering (DIIN), University of Salerno, 84084 Fisciano, Salerno, Italy*

Claudio Imparato − *Department of Chemical, Materials and Production Engineering (DICMaPI), University of Naples Federico II, 80125 Naples, Italy*; orcid.org/0000-0003-1725-7008

Marialuigia Raimondo − *Department of Industrial Engineering (DIIN), University of Salerno, 84084 Fisciano, Salerno, Italy*

Roberto Pantani − *Department of Industrial Engineering (DIIN), University of Salerno, 84084 Fisciano, Salerno, Italy*

Antonio Aronne − *Department of Chemical, Materials and Production Engineering (DICMaPI), University of Naples Federico II, 80125 Naples, Italy*; orcid.org/0000-0002-2711-6789

Liberata Guadagno − *Department of Industrial Engineering (DIIN), University of Salerno, 84084 Fisciano, Salerno, Italy*

Complete contact information is available at: https://pubs.acs.org/10.1021/acsomega.3c01415

Author Contributions

The manuscript was written through contributions of all authors. All authors have given approval to the final version of the manuscript.

Funding

This research is funded by the University of Salerno, project code: 300395CIC22RAIMONDO.

Notes

The authors declare no competing financial interest.

■ ACKNOWLEDGMENTS

The authors gratefully acknowledge the Department of Industrial Engineering of the University of Salerno, Italy (Department of Excellence 2023-2027, Italian Ministry of University and Research) for the financial support and the Organizing Committee of the 1st Congress of the Division "Chimica per le Tecnologie" of the Italian Chemical Society for the opportunity to plan the research activity. The authors would like to thank Dr. Valentina Roviello (Department of Chemical, Materials, and Production Engineering, University of Naples Federico II, Naples, Italy) for her support during SEM measurements.

■ REFERENCES

(1) Chen, H.; Wang, F.; Fan, H.; Hong, R.; Li, W. Construction of MOF-based superhydrophobic composite coating with excellent abrasion resistance and durability for self-cleaning, corrosion resistance, anti-icing, and loading-increasing research. *Chem. Eng. J.* **2021**, *408*, 127343.

(2) Zeng, D.; Li, Y.; Huan, D.; Liu, H.; Luo, H.; Cui, Y.; Zhu, C.; Wang, J. Robust epoxy-modified superhydrophobic coating for aircraft anti-icing systems. *Colloids Surf., A* **2021**, *628*, 127377.

(3) Javaid, S.; Mahmood, A.; Nasir, H.; Iqbal, M.; Ahmed, N.; Ahmad, N. M. Layer-By-Layer Self-Assembled Dip Coating for Antifouling Functionalized Finishing of Cotton Textile. *Polymers* **2022**, *14*, 2540.

(4) Yoon, J.; Ryu, M.; Kim, H.; Ahn, G. N.; Yim, S. J.; Kim, D. P.; Lee, H. Wet-style superhydrophobic antifogging coatings for optical sensors. *Adv. Mater.* **2020**, *32*, 2002710.

(5) Chen, H.; Fan, H.; Su, N.; Hong, R.; Lu, X. Highly hydrophobic polyaniline nanoparticles for anti-corrosion epoxy coatings. *Chem. Eng. J.* **2021**, *420*, 130540.

(6) Das, S.; Kumar, S.; Samal, S. K.; Mohanty, S.; Nayak, S. K. A review on superhydrophobic polymer nanocoatings: recent development and applications. *Ind. Eng. Chem. Res.* **2018**, *57*, 2727−2745.
(7) Brown, S.; Lengaigne, J.; Sharifi, N.; Pugh, M.; Moreau, C.; Dolatabadi, A.; Martinu, L.; Klemberg-Sapieha, J. E. Durability of superhydrophobic duplex coating systems for aerospace applications. *Surf. Coat. Technol.* **2020**, *401*, 126249.
(8) Lacruz, A.; Salvador, M.; Blanco, M.; Vidal, K.; Goitandia, A. M.; Martinková, L.; Kyselka, M.; de Ilarduya, A. M. Biobased Waterborne Polyurethane-Ureas Modified with POSS-OH for Fluorine-Free Hydrophobic Textile Coatings. *Polymers* **2021**, *13*, 3526.
(9) Kumar, R.; Kumar Sahani, A. Role of superhydrophobic coatings in biomedical applications. *Mater. Today: Proc.* **2021**, *45*, 5655−5659.
(10) Tinti, A.; Carallo, G. A.; Greco, A.; Romero-Sánchez, M. D.; Vertuccio, L.; Guadagno, L. Effective Practical Solutions for De-Icing of Automotive Component. *Nanomaterials* **2022**, *12*, 2979.
(11) Guadagno, L.; Vertuccio, L.; Foglia, F.; Raimondo, M.; Barra, G.; Sorrentino, A.; Pantani, R.; Calabrese, E. Flexible eco-friendly multilayer film heaters. *Composites, Part B* **2021**, *224*, 109208.
(12) Vertuccio, L.; Foglia, F.; Pantani, R.; Romero-Sánchez, M. D.; Calderón, B.; Guadagno, L. Carbon nanotubes and expanded graphite based bulk nanocomposites for de-icing applications. *Composites, Part B* **2021**, *207*, 108583.
(13) Kota, A. K.; Kwon, G.; Tuteja, A. The design and applications of superomniphobic surfaces. *NPG Asia Mater.* **2014**, *6*, No. e109.
(14) Sreekantan, S.; Yong, A. X.; Basiron, N.; Ahmad, F.; De'nan, F. Effect of Solvent on Superhydrophobicity Behavior of Tiles Coated with Epoxy/PDMS/SS. *Polymers* **2022**, *14*, 2406.
(15) Mahadik, S. A.; Kavale, M. S.; Mukherjee, S. K.; Rao, A. V. Transparent superhydrophobic silica coatings on glass by sol−gel method. *Appl. Surf. Sci.* **2010**, *257*, 333−339.
(16) Sharma, K.; Hooda, A.; Goyat, M. S.; Rai, R.; Mittal, A. A review on challenges, recent progress and applications of silica nanoparticles based superhydrophobic coatings. *Ceram. Int.* **2022**, *48*, 5922−5938.
(17) Chakradhar, R. P. S.; Kumar, V. D.; Rao, J. L.; Basu, B. J. Fabrication of superhydrophobic surfaces based on ZnO−PDMS nanocomposite coatings and study of its wetting behaviour. *Appl. Surf. Sci.* **2011**, *257*, 8569−8575.
(18) Lai, Y.; Tang, Y.; Gong, J.; Gong, D.; Chi, L.; Lin, C.; Chen, Z. Transparent superhydrophobic/superhydrophilic TiO 2-based coatings for self-cleaning and anti-fogging. *J. Mater. Chem.* **2012**, *22*, 7420−7426.
(19) Barati Darband, G.; Aliofkhazraei, M.; Khorsand, S.; Sokhanvar, S.; Kaboli, A. Science and engineering of superhydrophobic surfaces: review of corrosion resistance, chemical and mechanical stability. *Arabian J. Chem.* **2020**, *13*, 1763−1802.
(20) Ding, B.; Ogawa, T.; Kim, J.; Fujimoto, K.; Shiratori, S. Fabrication of a super-hydrophobic nanofibrous zinc oxide film surface by electrospinning. *Thin Solid Films* **2008**, *516*, 2495−2501.
(21) Burkarter, E.; Saul, C. K.; Thomazi, F.; Cruz, N. C.; Roman, L. S.; Schreiner, W. H. Superhydrophobic electrosprayed PTFE. *Surf. Coat. Technol.* **2007**, *202*, 194−198.
(22) Cai, Z.; Lin, J.; Hong, X. Transparent superhydrophobic hollow films (TSHFs) with superior thermal stability and moisture resistance. *RSC Adv.* **2018**, *8*, 491−498.
(23) Syed, J. A.; Tang, S.; Meng, X. Super-hydrophobic multilayer coatings with layer number tuned swapping in surface wettability and redox catalytic anti-corrosion application. *Sci. Rep.* **2017**, *7*, 4403−4417.
(24) Singh, A. K.; Singh, J. K. Fabrication of durable superhydrophobic coatings on cotton fabrics with photocatalytic activity by fluorine-free chemical modification for dual-functional water purification. *New J. Chem.* **2017**, *41*, 4618−4628.
(25) Jin, J.; Wang, X.; Song, M. Graphene-based nanostructured hybrid materials for conductive and superhydrophobic functional coatings. *J. Nanosci. Nanotechnol.* **2011**, *11*, 7715−7722.
(26) Passaro, J.; Imparato, C.; Parida, D.; Bifulco, A.; Branda, F.; Aronne, A. Electrospinning of PVP-based ternary composites containing SiO2 nanoparticles and hybrid TiO2 microparticles with adsorbed superoxide radicals. *Composites, Part B* **2022**, *238*, 109874.
(27) Salimian, S.; Zadhoush, A. Water-glass based silica aerogel: unique nanostructured filler for epoxy nanocomposites. *J. Porous Mater.* **2019**, *26*, 1755−1765.
(28) Li, Z.; Xing, Y.; Dai, J. Superhydrophobic surfaces prepared from water glass and non-fluorinated alkylsilane on cotton substrates. *Appl. Surf. Sci.* **2008**, *254*, 2131−2135.
(29) Shang, H. M.; Wang, Y.; Takahashi, K.; Cao, G. Z.; Li, D.; Xia, Y. N. Nanostructured superhydrophobic surfaces. *J. Mater. Sci.* **2005**, *40*, 3587−3591.
(30) Gu, G.; Dang, H.; Zhang, Z.; Wu, Z. Fabrication and characterization of transparent superhydrophobic thin films based on silica nanoparticles. *Appl. Phys. A* **2006**, *83*, 131−132.
(31) Bravo, J.; Zhai, L.; Wu, Z.; Cohen, R. E.; Rubner, M. F. Transparent superhydrophobic films based on silica nanoparticles. *Langmuir* **2007**, *23*, 7293−7298.
(32) Xue, C.-H.; Jia, S.-T.; Zhang, J.; Tian, L.-Q. Superhydrophobic surfaces on cotton textiles by complex coating of silica nanoparticles and hydrophobization. *Thin Solid Films* **2009**, *517*, 4593−4598.
(33) Mazari, S. A.; Mubarak, N. M.; Jatoi, A. S.; Abro, R.; Shah, A.; Shah, A. K.; Sabzoi, N.; Baloch, H.; Kumar, V.; Lghari, Z. Environmental impact of using nanomaterials in textiles. *Nanosensors and nanodevices for smart multifunctional textiles*; Elsevier, 2021; pp 321−342.
(34) Wang, S.; Guo, X.; Xie, Y.; Liu, L.; Yang, H.; Zhu, R.; Gong, J.; Peng, L.; Ding, W. Preparation of superhydrophobic silica film on Mg−Nd−Zn−Zr magnesium alloy with enhanced corrosion resistance by combining micro-arc oxidation and sol−gel method. *Surf. Coat. Technol.* **2012**, *213*, 192−201.
(35) Glüge, J.; Scheringer, M.; Cousins, I. T.; DeWitt, J. C.; Goldenman, G.; Herzke, D.; Lohmann, R.; Ng, C. A.; Trier, X.; Wang, Z. An overview of the uses of per-and polyfluoroalkyl substances (PFAS). *Environmental Science: Processes & Impacts* **2020**, *22*, 2345−2373.
(36) Cousins, I. T.; Johansson, J. H.; Salter, M. E.; Sha, B.; Scheringer, M. Outside the safe operating space of a new planetary boundary for per-and polyfluoroalkyl substances (PFAS). *Environ. Sci. Technol.* **2022**, *56*, 11172−11179.
(37) Penna, M. O.; Silva, A. A.; do Rosario, F. F.; De Souza Camargo, S.; Soares, B. G. Organophilic nano-alumina for superhydrophobic epoxy coatings. *Mater. Chem. Phys.* **2020**, *255*, 123543.
(38) Jiao, Z.; Chu, W.; Liu, L.; Mu, Z.; Li, B.; Wang, Z.; Liao, Z.; Wang, Y.; Xue, H.; Niu, S.; et al. Underwater writable and heat-insulated paper with robust fluorine-free superhydrophobic coatings. *Nanoscale* **2020**, *12*, 8536−8545.
(39) Jin, H.; Tian, X.; Ikkala, O.; Ras, R. H. A. Preservation of superhydrophobic and superoleophobic properties upon wear damage. *ACS Appl. Mater. Interfaces* **2013**, *5*, 485−488.
(40) Jin, F.-L.; Li, X.; Park, S.-J. Synthesis and application of epoxy resins: A review. *J. Ind. Eng. Chem.* **2015**, *29*, 1−11.
(41) Psarski, M.; Celichowski, G.; Marczak, J.; Gumowski, K.; Sobieraj, G. B. Superhydrophobic dual-sized filler epoxy composite coatings. *Surf. Coat. Technol.* **2013**, *225*, 66−74.
(42) Psarski, M.; Marczak, J.; Celichowski, G.; Sobieraj, G. B.; Gumowski, K.; Zhou, F.; Liu, W. Hydrophobization of epoxy nanocomposite surface with 1H, 1H, 2H, 2H-perfluorooctyltrichlorosilane for superhydrophobic properties. *Cent. Eur. J. Phys.* **2012**, *10*, 1197−1201.
(43) Hill, D.; Barron, A. R.; Alexander, S. Comparison of hydrophobicity and durability of functionalized aluminium oxide nanoparticle coatings with magnetite nanoparticles−links between morphology and wettability. *J. Colloid Interface Sci.* **2019**, *555*, 323−330.
(44) Ma, T.; Ma, J.; Yang, C.; Zhang, J.; Cheng, J. Robust, multiresponsive, superhydrophobic, and oleophobic nanocomposites via a highly efficient multifluorination strategy. *ACS Appl. Mater. Interfaces* **2021**, *13*, 28949−28961.

https://doi.org/10.1021/acsomega.3c01415
ACS Omega 2023, 8, 23596−23606

(45) Zhong, M.; Zhang, Y.; Li, X.; Wu, X. Facile fabrication of durable superhydrophobic silica/epoxy resin coatings with compatible transparency and stability. *Surf. Coat. Technol.* **2018**, *347*, 191−198.
(46) Cai, C.; Sang, N.; Teng, S.; Shen, Z.; Guo, J.; Zhao, X.; Guo, Z. Superhydrophobic surface fabricated by spraying hydrophobic R974 nanoparticles and the drag reduction in water. *Surf. Coat. Technol.* **2016**, *307*, 366−373.
(47) Wu, B.; Lyu, J.; Peng, C.; Jiang, D.; Yang, J.; Yang, J.; Xing, S.; Sheng, L. Inverse infusion processed hierarchical structure towards superhydrophobic coatings with ultrahigh mechanical robustness. *Chem. Eng. J.* **2020**, *387*, 124066.
(48) Holbery, J.; Houston, D. Natural-fiber-reinforced polymer composites in automotive applications. *Jom* **2006**, *58*, 80−86.
(49) Viscusi, G.; Barra, G.; Verdolotti, L.; Galzerano, B.; Viscardi, M.; Gorrasi, G. Natural fiber reinforced inorganic foam composites from short hemp bast fibers obtained by mechanical decortation of unretted stems from the wastes of hemp cultivations. *Mater. Today: Proc.* **2021**, *34*, 176−179.
(50) Raju, P.; Raja, K.; Lingadurai, K.; Maridurai, T.; Prasanna, S. C. Glass/Caryota urens hybridized fibre-reinforced nanoclay/SiC toughened epoxy hybrid composite: mechanical, drop load impact, hydrophobicity and fatigue behaviour. *Biomass Convers. Biorefin.* **2021**, *13*, 1143−1152.
(51) Alshahrani, H.; Pathinettampadian, G.; Gujba, A. K.; Prakash Vincent Rethnam, A. Effect of palmyra sprout fiber and biosilica on mechanical, wear, thermal and hydrophobic behavior of epoxy resin composite. *J. Ind. Text.* **2022**, *52*, 152808372211373.
(52) Doan, T. T. L.; Brodowsky, H.; Mäder, E. Jute fibre/epoxy composites: Surface properties and interfacial adhesion. *Compos. Sci. Technol.* **2012**, *72*, 1160−1166.
(53) Yang, G.; Park, M.; Park, S.-J. Recent progresses of fabrication and characterization of fibers-reinforced composites: A review. *Compos. Commun.* **2019**, *14*, 34−42.
(54) Paiva, J. M. F. d.; Santos, A. D. N. d.; Rezende, M. C. Mechanical and morphological characterizations of carbon fiber fabric reinforced epoxy composites used in aeronautical field. *Mater. Res.* **2009**, *12*, 367−374.
(55) Bifulco, A.; Silvestri, B.; Passaro, J.; Boccarusso, L.; Roviello, V.; Branda, F.; Durante, M. A New Strategy to Produce Hemp Fibers through a Waterglass-Based Ecofriendly Process. *Materials* **2020**, *13*, 1844.
(56) Branda, F.; Malucelli, G.; Durante, M.; Piccolo, A.; Mazzei, P.; Costantini, A.; Silvestri, B.; Pennetta, M.; Bifulco, A. Silica treatments: A fire retardant strategy for hemp fabric/epoxy composites. *Polymers* **2016**, *8*, 313.
(57) Avossa, J.; Bifulco, A.; Amendola, E.; Gesuele, F.; Oscurato, S. L.; Gizaw, Y.; Mensitieri, G.; Branda, F. Forming nanostructured surfaces through Janus colloidal silica particles with nanowrinkles: A new strategy to superhydrophobicity. *Appl. Surf. Sci.* **2019**, *465*, 73−81.
(58) Hilal, N.; Ismail, A. F.; Matsuura, T.; Oatley-Radcliffe, D. *Membrane characterization*; Elsevier, 2017.
(59) Nobile, M. R.; Raimondo, M.; Naddeo, C.; Guadagno, L. Rheological and morphological properties of non-covalently functionalized graphene-based structural epoxy resins with intrinsic electrical conductivity and thermal stability. *Nanomaterials* **2020**, *10*, 1310.
(60) Pinto, D.; Amaro, A. M.; Bernardo, L. Experimental study on the surface properties of nanoalumina-filled epoxy resin nanocomposites. *Appl. Sci.* **2020**, *10*, 733.
(61) Wenzel, R. N. Resistance of solid surfaces to wetting by water. *Ind. Eng. Chem.* **1936**, *28*, 988−994.
(62) Thakur, V. K. *Lignocellulosic polymer composites: Processing, characterization, and properties*; John Wiley & Sons, 2014.
(63) Branda, F.; Bifulco, A.; Jehnichen, D.; Parida, D.; Pauer, R.; Passaro, J.; Gaan, S.; Pospiech, D.; Durante, M. Structure and Bottom-up Formation Mechanism of Multisheet Silica-Based Nanoparticles Formed in an Epoxy Matrix through an In Situ Process. *Langmuir* **2021**, *37*, 8886−8893.
(64) Sun, Z.; Wong, R.; Yu, M.; Li, J.; Zhang, M.; Mele, L.; Hah, J.; Kathaperumal, M.; Wong, C.-P. Nanocomposites for future electronics device Packaging: A fundamental study of interfacial connecting mechanisms and optimal conditions of silane coupling agents for Polydopamine-Graphene fillers in epoxy polymers. *Chem. Eng. J.* **2022**, *439*, 135621.
(65) Wang, B.; Sain, M.; Oksman, K. Study of structural morphology of hemp fiber from the micro to the nanoscale. *Appl. Compos. Mater.* **2007**, *14*, 89−103.
(66) Panaitescu, D. M.; Vuluga, Z.; Ghiurea, M.; Iorga, M.; Nicolae, C.; Gabor, R. Influence of compatibilizing system on morphology, thermal and mechanical properties of high flow polypropylene reinforced with short hemp fibers. *Composites, Part B* **2015**, *69*, 286−295.
(67) Guadagno, L.; Longo, P.; Raimondo, M.; Naddeo, C.; Mariconda, A.; Sorrentino, A.; Vittoria, V.; Iannuzzo, G.; Russo, S. Cure behavior and mechanical properties of structural self-healing epoxy resins. *J. Polym. Sci., Part B: Polym. Phys.* **2010**, *48*, 2413−2423.
(68) Xu, Y. l.; Dayo, A. Q.; Wang, J.; Wang, A. r.; Lv, D.; Zegaoui, A.; Derradji, M.; Liu, W. b. Mechanical and thermal properties of a room temperature curing epoxy resin and related hemp fibers reinforced composites using a novel in-situ generated curing agent. *Mater. Chem. Phys.* **2018**, *203*, 293−301.
(69) Gargol, M.; Klepka, T.; Klapiszewski, Ł.; Podkościelna, B. Synthesis and thermo-mechanical study of epoxy resin-based composites with waste fibers of hemp as an eco-friendly filler. *Polymers* **2021**, *13*, 503.
(70) Aronne, A.; Marenna, E.; Califano, V.; Fanelli, E.; Pernice, P.; Trifuoggi, M.; Vergara, A. Sol−gel synthesis and structural characterization of niobium-silicon mixed-oxide nanocomposites. *J. Sol-Gel Sci. Technol.* **2007**, *43*, 193−204.
(71) Hameed, N.; Guo, Q.; Hanley, T.; Mai, Y. W. Hydrogen bonding interactions, crystallization, and surface hydrophobicity in nanostructured epoxy/block copolymer blends. *J. Polym. Sci., Part B: Polym. Phys.* **2010**, *48*, 790−800.
(72) Bellido-Aguilar, D. A.; Zheng, S.; Huang, Y.; Zeng, X.; Zhang, Q.; Chen, Z. Solvent-free synthesis and hydrophobization of biobased epoxy coatings for anti-icing and anticorrosion applications. *ACS Sustainable Chem. Eng.* **2019**, *7*, 19131−19141.
(73) Ma, L.; Wang, J.; Zhang, D.; Huang, Y.; Huang, L.; Wang, P.; Qian, H.; Li, X.; Terryn, H. A.; Mol, J. M. C. Dual-action self-healing protective coatings with photothermal responsive corrosion inhibitor nanocontainers. *Chem. Eng. J.* **2021**, *404*, 127118.
(74) Qian, H.; Liu, B.; Wu, D.; Zhang, F.; Wang, X.; Jin, L.; Wang, J.; Zhang, D.; Li, X. Magnetically responsive lubricant-infused porous surfaces with controllable lubricity and durable anti-icing performance. *Surf. Coat. Technol.* **2021**, *406*, 126742.
(75) Ou, J.; Shi, Q.; Wang, Z.; Wang, F.; Xue, M.; Li, W.; Yan, G. Sessile droplet freezing and ice adhesion on aluminum with different surface wettability and surface temperature. *Sci. China: Phys., Mech. Astron.* **2015**, *58*, 1−8.
(76) Sadasivuni, K. K.; Saiter, A.; Gautier, N.; Thomas, S.; Grohens, Y. Effect of molecular interactions on the performance of poly (isobutylene-co-isoprene)/graphene and clay nanocomposites. *Colloid Polym. Sci.* **2013**, *291*, 1729−1740.
(77) Zhuo, Y.; Li, T.; Wang, F.; Håkonsen, V.; Xiao, S.; He, J.; Zhang, Z. An ultra-durable icephobic coating by a molecular pulley. *Soft Matter* **2019**, *15*, 3607−3611.
(78) Irajizad, P.; Nazifi, S.; Ghasemi, H. Icephobic surfaces: Definition and figures of merit. *Sci. China: Phys., Mech. Astron.* **2019**, *269*, 203−218.
(79) Prado, L. A. S. D. A.; De La Vega, A.; Sumfleth, J.; Schulte, K. Noncovalent functionalization of multiwalled and double-walled carbon nanotubes: Positive effect of the filler functionalization on high glass transition temperature epoxy resins. *J. Polym. Sci., Part B: Polym. Phys.* **2009**, *47*, 1860−1868.
(80) Guadagno, L.; Vertuccio, L.; Naddeo, C.; Calabrese, E.; Barra, G.; Raimondo, M.; Sorrentino, A.; Binder, W. H.; Michael, P.; Rana,

https://doi.org/10.1021/acsomega.3c01415
ACS Omega 2023, 8, 23596−23606

S. Reversible self-healing carbon-based nanocomposites for structural applications. *Polymers* **2019**, *11*, 903.
(81) Guadagno, L.; Vertuccio, L.; Barra, G.; Naddeo, C.; Sorrentino, A.; Lavorgna, M.; Raimondo, M.; Calabrese, E. Eco-friendly polymer nanocomposites designed for self-healing applications. *Polymer* **2021**, *223*, 123718.
(82) Guadagno, L.; Raimondo, M.; Naddeo, C.; Vertuccio, L.; Russo, S.; Iannuzzo, G.; Calabrese, E. Rheological, Thermal and Mechanical Characterization of Toughened Self-Healing Supramolecular Resins, Based on Hydrogen Bonding. *Nanomaterials* **2022**, *12*, 4322.
(83) Liparoti, S.; Pantani, R.; Sorrentino, A.; Speranza, V.; Titomanlio, G. Hydrophobicity tuning by the fast evolution of mold temperature during injection molding. *Polymers* **2018**, *10*, 322.

https://doi.org/10.1021/acsomega.3c01415
ACS Omega 2023, 8, 23596−23606